



# Spin transport in noncollinear antiferromagnetic metals

Yihong Cheng  and Shufeng Zhang *Department of Physics, University of Arizona, Tucson, Arizona 85721, USA*

(Received 21 January 2020; revised 1 June 2020; accepted 20 September 2020; published 5 October 2020)

For noncollinear antiferromagnetic metals, magnon spectra display nontrivial multiband structure in which both direction and magnitude of the angular momenta of magnons are momentum dependent. We study the roles of these magnons on the spin transport properties by taking into account the momentum and angular momentum transfer between conduction electrons and magnons. We have calculated spin conductivity tensor by using the coupled Boltzmann equations for the electron spin and magnon, and we show that the unpolarized electron current driven by an electric field can efficiently induce a magnon spin current. The temperature dependence of the magnon spin conductivity is also calculated.

DOI: [10.1103/PhysRevB.102.134403](https://doi.org/10.1103/PhysRevB.102.134403)

## I. INTRODUCTION

Antiferromagnets (AFMs) are of great interest for the study of spintronics recently [1–4]. Most studies on spin transport phenomena so far have focused on collinear AFMs, i.e., two magnetic sublattices have an opposite direction of magnetic moments. For example, the spin Seebeck [5–8] and spin pumping effects [9,10] in AFMs, the magnon transfer torque in ferromagnet (FM)/AFM/FM sandwich structure [11–13], and spin Hall effect in AFMs [14,15]. More recently, the noncollinear AFMs have shown qualitatively and quantitatively different transport properties compared to those of collinear AFMs. The noncollinear antiferromagnetic system  $\text{Mn}_3\text{Z}$  ( $\text{Z} = \text{Sn}, \text{Ir}, \text{and Ge}$ ) has been found to have a strong anomalous Hall effect [16–19] compared to ferromagnetic metals. The interfacial spin transfer between noncollinear AFMs and normal metals has been theoretically demonstrated [20]. In insulating noncollinear AFMs, studies have established evidence of the thermal Hall effect [21,22] and the spin Seebeck and spin Nernst effects [23]. Also, the spin Hall and inverse spin Hall effects [24,25] have been reported in  $\text{Mn}_3\text{Sn}$ , where previous research has focused mainly on nonmagnetic heavy metals.

For a collinear AFM, one may define a Néel vector, representing the difference between two antiparallel magnetic moments of two sublattices. The magnons, which are quasi-particles of the low-energy excitations, are then quantized in the direction either parallel or antiparallel to the Néel vector, i.e., the magnon spectra have two doubly degenerated branches with each magnon's angular momentum either parallel or antiparallel to the Néel vector. In this case, the spin direction of the magnon is fixed by the Néel vector, independent of the momentum of the magnon. For noncollinear AFMs, however, the Néel vectors cannot be defined by a single vector. In fact, we will show that each magnon is no longer an eigenstate of the spin angular momentum. The average magnitude and direction of the angular momentum depend on the momentum of the magnon [26].

The above spin-momentum locking of magnons would strongly affect the electrical and magnetoelectrical transport properties of noncollinear antiferromagnetic metals. Magnons and conduction electrons are two main angular momentum carriers that determine the total spin current. Although an applied electric field only drives the charge current of the conduction electrons, the magnon current can be induced by electron-magnon scattering such that the electron transfers its momentum to the magnons [27]. The resulting net momentum of magnons, along with the intrinsic angular momentum of each magnon, generates a magnon spin current. In this paper, we show that the novel types of magnon spin currents can be efficiently generated by purely electrical means in noncollinear AFMs. The paper is organized as follows. In Sec. II, we propose a two-dimensional spin Hamiltonian of a kagome lattice with nearest antiferromagnetic exchange interaction, including a Dzyaloshinskii-Moriya interaction (DMI) and an on-site anisotropic term. We solve the magnon spectra of the Hamiltonian and determine the spin-momentum locking pattern in momentum space. In Sec. III, we propose an exchange Hamiltonian between the conduction electrons and local spins of the noncollinear AFMs, and calculate the magnon spin current under external electric field. In Sec. IV, we discuss the key results of this paper.

## II. MAGNON BANDS AND SPIN-MOMENTUM LOCKING

We start with a two-dimensional (2D) kagome antiferromagnetic metal, consisting of the unpolarized conduction electrons and local magnetic spins. The antiferromagnetic exchange coupling of the local spins yields a classical spin-fluctuation ground state in which the spins in the three sublattices  $\mathbf{S}_A$ ,  $\mathbf{S}_B$ , and  $\mathbf{S}_C$ , form  $120^\circ$  angles to each other, as shown in Fig. 1(a). Note that the ground state is highly degenerate with a number of different spin configurations if the isotropic antiferromagnetic exchange coupling is the only spin Hamiltonian. To freeze the ground state spin configurations, we include two additional anisotropic terms to model

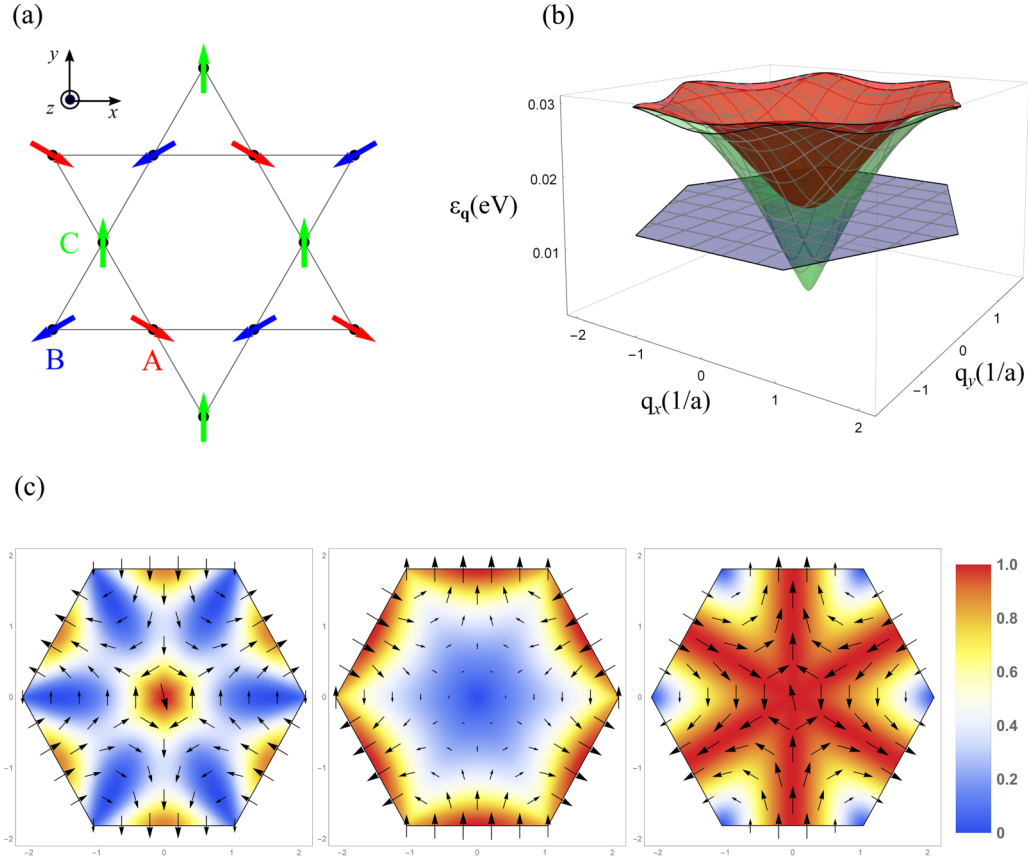


FIG. 1. (a) The kagome antiferromagnetic lattice with three sublattices, labeled A, B, and C. (b) The magnon dispersion relations in the first Brillouin zone. Here the parameters are as follows:  $J_{\text{ex}} = 10$  meV,  $D_z = 1/10J_{\text{ex}}$ ,  $K = 1/1000J_{\text{ex}}$ , and  $S = 5/2$ . At small  $\mathbf{q}$ , the red band is quadratic, the green band is linear, and the blue band is finite and flat over the entire first Brillouin zone. Note the red band and blue band touch each other at  $\mathbf{q} = 0$ . (c) The  $\mathbf{q}$ -resolved magnon spins. From the left to right: red, green, and blue bands. The arrow at a given point of the magnon bands represents the direction of the expectation value of the magnon spin,  $\mathbf{S}_{\nu\mathbf{q}} = \langle \nu\mathbf{q} | \sum_{i\alpha} \mathbf{S}_{i\alpha} | \nu\mathbf{q} \rangle$ , and the color assignment is for its magnitude  $|\mathbf{S}_{\nu\mathbf{q}}|/S$ .

the Hamiltonian [28–30],

$$\hat{H} = \sum_{\langle i,j \rangle} [J_{\text{ex}} \mathbf{S}_i \cdot \mathbf{S}_j + \mathbf{D}_{ij} \cdot (\mathbf{S}_i \times \mathbf{S}_j)] - K \sum_i (\mathbf{S}_i \cdot \mathbf{z}'_i)^2, \quad (1)$$

where  $\langle i, j \rangle$  is the summation over nearest neighbors,  $J_{\text{ex}} > 0$  is the antiferromagnetic Heisenberg exchange,  $\mathbf{D}_{ij} = D_z \hat{\mathbf{z}}$  is the DMI which is assumed perpendicular to the 2D plane, and  $K$  is the single-ion anisotropy with the anisotropic axis  $\mathbf{z}'_i$  defined as the unit vector whose direction is parallel to the spin orientations of the frozen classical ground state [see Fig. 1(a)]. We should point out that these anisotropy terms are essential for the antiferromagnetic ground state since the theorem of Mermin and Wagner [31] would exclude the long-range antiferromagnetic ordering for an isotropic exchange Hamiltonian. We have taken the above anisotropic terms which have already been used [21, 26, 28–30], and we assume that both  $D_{ij}$  and  $K$  are much smaller than  $J_{\text{ex}}$ . The other part of the Hamiltonian involves the interaction between conduction electrons and the local spins, which will be explicitly included when we discuss the magnon spin conductivity. In this section, we shall determine the low-energy excitations from Eq. (1), i.e., the magnon dispersions or the magnon bands.

Following the conventional linear spin-wave approach, we introduce the Holstein-Primakoff (HP) transformation

$$\begin{aligned} \mathbf{S}_{i\alpha} = & \mathbf{z}'_{i\alpha} (S - b_{i\alpha}^\dagger b_{i\alpha}) + \mathbf{x}'_{i\alpha} \sqrt{\frac{S}{2}} (b_{i\alpha} + b_{i\alpha}^\dagger) \\ & - \mathbf{y}'_{i\alpha} i \sqrt{\frac{S}{2}} (b_{i\alpha} - b_{i\alpha}^\dagger), \end{aligned} \quad (2)$$

where  $S$  is the spin,  $b_{i\alpha}^\dagger$  ( $b_{i\alpha}$ ) is the magnon creation (annihilation) operator of the sublattice  $\alpha$  ( $\alpha = A, B, C$ ) at unit cell  $i$ , and  $\mathbf{x}'_{i\alpha}, \mathbf{y}'_{i\alpha}, \mathbf{z}'_{i\alpha}$  denotes the local Cartesian coordinate system. By replacing Eq. (2) with (1), and discarding terms with more than the second order in the HP bosons, we find, after Fourier transformation, the spin Hamiltonian can be written in a compact form [26, 32],

$$\hat{H} = \sum_{\mathbf{q}} (b_{\mathbf{q}}^\dagger \ b_{-\mathbf{q}}) \cdot H(\mathbf{q}) \cdot \begin{pmatrix} b_{\mathbf{q}} \\ b_{-\mathbf{q}}^\dagger \end{pmatrix}, \quad (3)$$

where  $b_{\mathbf{q}}^\dagger = (b_{A\mathbf{q}}^\dagger \ b_{B\mathbf{q}}^\dagger \ b_{C\mathbf{q}}^\dagger)$  and  $H(\mathbf{q})$  is a  $6 \times 6$  bosonic Bogoliubov–de Gennes matrix whose explicit expression is rather cumbersome, but it was straightforwardly obtained by simple but tedious algebra. To obtain the eigenenergies and eigenstates, we need to diagonalize the matrix  $H(\mathbf{q})$ .

A standard procedure is to carry the Bogoliubov transformation, i.e.,

$$b_{\alpha\mathbf{q}} = \sum_{\nu} (M_{\nu\mathbf{q}}^{\alpha} b_{\nu\mathbf{q}} + N_{\nu\mathbf{q}}^{\alpha} b_{\nu-\mathbf{q}}^{\dagger}), \quad (4)$$

where  $\nu = 1, 2, 3$  represents three band indices. By placing Eq. (4) into (3), and by utilizing the commutator properties of the boson operators, we numerically determine the transformation matrices  $M_{\nu\mathbf{q}}^{\alpha}$  and  $N_{\nu\mathbf{q}}^{\alpha}$  and obtain the diagonalized Hamiltonian,

$$\hat{H} = \sum_{\nu\mathbf{q}} \varepsilon_{\nu\mathbf{q}} b_{\nu\mathbf{q}}^{\dagger} b_{\nu\mathbf{q}}, \quad (5)$$

where  $\varepsilon_{\nu\mathbf{q}}$  is the magnon dispersion relation. The three magnon dispersions in the first Brillouin zone are shown in Fig. 1(b) where three branches of the magnons are color-coded with red, green, and blue. Interestingly, for small wave number  $\mathbf{q}$ , the red band is quadratic, the green band is linear, and the blue is a flatband with finite energy. Note that the Goldstone mode, which is the zero-energy mode of bosons, does not show up in any of the three magnon bands since we introduce an anisotropy in Eq. (1), i.e., the magnons are gapped at  $\mathbf{q} = 0$ .

In collinear AFMs, two band indices represent the magnon spin state, i.e., the magnon in one band has the angular momentum parallel to the Néel vector and in the other band, antiparallel to the Néel vector. In the present case, the transformation to diagonalize the matrix  $H(\mathbf{q})$ , Eq. (4), mixes spin states in three sublattices. Consequently, the magnons in three bands are no longer an eigenstate of the angular momentum. To determine the angular momentum transfer between conduction electrons and magnons in the next section, we define the spin of a magnon by its average value of all spins,

$$\mathbf{S}_{\nu\mathbf{q}} = \langle \nu\mathbf{q} | \sum_{i\alpha} \mathbf{S}_{i\alpha} | \nu\mathbf{q} \rangle, \quad (6)$$

where  $|\nu\mathbf{q}\rangle$  is the wave function of the magnon. In Fig. 1(c) we show the  $\mathbf{q}$ -dependent magnon spin for the three bands. For a given magnon  $b_{\nu\mathbf{q}}^{\dagger}$ , its spin direction is uniquely defined. We shall emphasize that the spin-momentum locking for magnons differs from that for conventional Rashba-like conduction electrons in two aspects: (1) The electron spins are locked in the direction perpendicular to the momentum for Rashba spin-orbit coupling (for more complicated spin-orbit coupling, the momentum-spin locking may take different patterns) while the magnon spins have a wide range of angle distribution relative to the magnon momentum, and (2) both spin and momentum are good quantum numbers (eigenstate) for conduction electrons in the Rashba spin-orbit coupled system, while for noncollinear antiferromagnetic magnons, only momentum, but not spin, is the good quantum number. Consequently, the magnitude of the spin for different magnons is different and is no longer quantized, as illustrated in Fig. 1(c).

### III. ELECTRON-MAGNON SCATTERING AND MAGNON SPIN CONDUCTIVITY

To study the roles of the above magnons in charge and spin transport, we consider the conduction electrons interacting

with magnons via  $s$ - $d$  exchange coupling given below:

$$\hat{H}_{sd} = -J_{sd} \sum_{i\alpha} \boldsymbol{\sigma}_{i\alpha} \cdot \mathbf{S}_{i\alpha}, \quad (7)$$

where  $J_{sd}$  is the  $s$ - $d$  exchange coupling,  $\boldsymbol{\sigma}$  is the electron spin, and indices  $i$  and  $\alpha$  are similarly defined as previously. The second quantized form of electron-magnon coupling can be further derived as [20]

$$\hat{H}_{sd} = \sum_{\sigma\sigma'\nu\mathbf{q}\mathbf{k}} \sum_{n=1}^3 [V_{\nu\mathbf{q}}^{(n)} b_{\nu\mathbf{q}}^{\dagger} c_{\mathbf{k}-\mathbf{q}\sigma'}^{\dagger} L_{\sigma'\sigma}^{(n)} c_{\mathbf{k}\sigma} + \text{H.c.}], \quad (8)$$

where  $c_{\mathbf{k}}^{\dagger}$  ( $c_{\mathbf{k}}$ ) is the electron creation (annihilation) operator,  $L_{\sigma'\sigma} = \{\sigma^{++} + \sigma^{-}, \sigma^{+} - \sigma^{-}, 2\sigma^z\}$ , and the coupling strength is

$$V_{\nu\mathbf{q}}^{(n)} = -\sqrt{2S}J_{sd} \sum_{\alpha} e^{i\mathbf{q}\cdot\boldsymbol{\delta}_{\alpha}} \times (f_{n\alpha}^{*} M_{\nu\mathbf{q}}^{\alpha} + f_{n\alpha} N_{\nu-\mathbf{q}}^{\alpha}) \quad (9)$$

where  $\boldsymbol{\delta}_{\alpha}$  is the position of the  $\alpha$ th site within the unit cell,  $f_{1\alpha} = \sin \theta_{\alpha}$ ,  $f_{2\alpha} = i \cos \theta_{\alpha}$ ,  $f_{3\alpha} = 2i$ , and  $\theta_{\alpha}$  is the angle of the classical orientation of the  $\alpha$ th site spin in global frame of reference.

Magnons are quasiparticles without electric charges and thus an applied electric field cannot directly drive magnon current. We have shown previously that the magnon can obtain its spin current in two essential ways: spin transfer and momentum transfer from conduction electrons to magnons [27]. As in the case of ferromagnetic metals, the electrons are spin polarized and thus there is always a magnon spin current in addition to the electron spin current [27]. If the conduction electron is not spin polarized, e.g., a collinear antiferromagnetic metal, the electron-magnon scattering would not lead to magnon spin current since the magnon momentum is independent of the spin and thus the sum over two degenerate magnon modes remains zero. In the present case, however, the spin and the momentum of magnons in the noncollinear AFMs are locked and therefore, the transferred momentum from the conduction electrons could generate magnon spin current. More quantitatively, we use Boltzmann transport formalism of the electrons and magnons to estimate the induced magnon spin current under an external electric field. We assume that the charge current is spin unpolarized for simplicity so that we discard the spin angular momentum transfer.

The magnon Boltzmann equation with the relaxation-time approximation is [6,27,33,34]

$$0 = -\frac{N_{\nu}(\mathbf{q}) - N_{\nu}^0(\mathbf{q})}{\tau_{\nu}} + \left( \frac{\partial N_{\nu}(\mathbf{q})}{\partial t} \right)_{sd}, \quad (10)$$

where  $N_{\nu}(\mathbf{q})$  is the magnon distribution function,  $\tau_{\nu}$  is the magnon relaxation time due to sources other than electrons, and  $(\frac{\partial N_{\nu}(\mathbf{q})}{\partial t})_{sd}$  is the electron-magnon scattering term which provides the nonequilibrium magnon distribution [27,33].

We separate the magnon distribution function into equilibrium and nonequilibrium parts

$$N_{\nu}(\mathbf{q}) = N_{\nu}^0(\mathbf{q}) + \frac{\partial N_{\nu}^0}{\partial \varepsilon_{\nu\mathbf{q}}} g_{\nu}(\mathbf{q}), \quad (11)$$

where  $g_{\nu}(\mathbf{q})$  is the nonequilibrium part that is going to be solved.

The electron-magnon scattering term is calculated via the Fermi golden rule

$$\left(\frac{\partial N_v(\mathbf{q})}{\partial t}\right)_{\text{sd}} = W_{v\mathbf{q}} \sum_{\mathbf{k}} \delta(\epsilon_{\mathbf{k}+\mathbf{q}} - \epsilon_{\mathbf{k}} - \epsilon_{v\mathbf{q}}) \times \{[N_v(\mathbf{q}) + 1][1 - f(\mathbf{k})]f(\mathbf{k} + \mathbf{q}) - N_v(\mathbf{q})[1 - f(\mathbf{k} + \mathbf{q})]f(\mathbf{k})\}, \quad (12)$$

where  $f(\mathbf{k})$  is the electron distribution function, and the scattering magnitude is

$$W_{v\mathbf{q}} = \frac{\pi}{\hbar} \sum_{n=1}^3 |V_{v\mathbf{q}}^{(n)}|^2. \quad (13)$$

The electron distribution satisfies the Boltzmann equation in which the scattering terms include the electron-magnon scattering and other scattering contributions such as impurities and phonons. In principle, one needs to self-consistently determine  $f(\mathbf{k})$  along with the magnon distribution. However, we will take a simplified approach by assuming one single relaxation time  $\tau_e$  as a parameter to represent all scatterings,

$$f(\mathbf{k}) = f^0(\mathbf{k}) - \frac{\partial f^0}{\partial \epsilon_{\mathbf{k}}} \frac{e\hbar\tau_e}{m} (\mathbf{E} \cdot \mathbf{k}), \quad (14)$$

where  $e$  is the electron charge,  $m$  is the electron mass,  $\epsilon_{\mathbf{k}}$  is the electron energy, and  $\mathbf{E}$  is the electric field. There are a number of justifications for our approximations. First, the effect of the electron-magnon scattering may not be more important for the conduction electrons compared to other sources of scattering. Second, the simple electron distribution allows us to reduce the mathematical complication in obtaining the magnon spin current.

By placing the electron distribution, Eq. (14), into the magnon's Boltzmann function, Eq. (10), we find the nonequilibrium part of magnons is

$$g_v(\mathbf{q}) = -\frac{1}{(1 + \frac{\tau_v^{\text{em}}(\mathbf{q})}{\tau_v})} \frac{e\hbar\tau_e}{m} (\mathbf{E} \cdot \mathbf{q}), \quad (15)$$

where the momentum-resolved electron-magnon relaxation time for magnons is

$$\tau_v^{\text{em}}(\mathbf{q}) = \frac{N_v^0(\mathbf{q})[N_v^0(\mathbf{q}) + 1]}{W_{v\mathbf{q}}\Gamma_{v\mathbf{q}}} \quad (16)$$

with

$$\Gamma_{v\mathbf{q}} = \sum_{\mathbf{k}} N_v^0(\mathbf{q})[1 - f^0(\mathbf{k} + \mathbf{q})]f^0(\mathbf{k}) \times \delta(\epsilon_{\mathbf{k}+\mathbf{q}} - \epsilon_{\mathbf{k}} - \epsilon_{v\mathbf{q}}). \quad (17)$$

The magnon spin current is then

$$(J_m)_j^i = \sum_{v\mathbf{q}} \frac{\partial N_v^0}{\partial \epsilon_{v\mathbf{q}}} g_v(\mathbf{q}) v_{v\mathbf{q}}^j S_{v\mathbf{q}}^i \equiv (\sigma_m)_{jk}^i E_k, \quad (18)$$

where  $i$  ( $j$ ) stands for the polarization (flow) direction of magnon spin current,  $k$  is the electric field direction,  $v$  is the magnon velocity, and  $\sigma_m$  is the magnon spin conductivity (similarly defined as electron spin conductivity). The magnon spin conductivity increases with the exchange coupling constant  $J_{\text{sd}}$  (it will be saturated for a large  $J_{\text{sd}}$  since the magnon

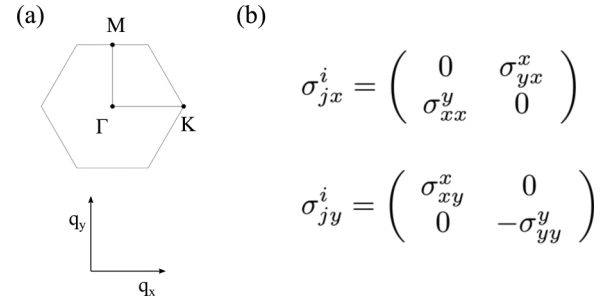


FIG. 2. (a) First Brillouin zone of the kagome AFM. Two high-symmetry axes are indicated with  $\Gamma K$  and  $\Gamma M$ . (b) The symmetry determined magnon spin conductivity tensor for  $\Gamma K$  and  $\Gamma M$  directions. The tensor  $(\sigma_m)_{jx}^i$  is off-diagonal while  $(\sigma_m)_{jy}^i$  is diagonal.

spin current comes from the electron spins via the exchange coupling). Specifically, the magnon conductivity scales with  $\tau_v J_{\text{sd}}^2 / (1 + \tau_v J_{\text{sd}}^2)$ .

Since the spin-momentum locking is complex, an electric field applied in an arbitrary direction relative to the crystal structure would generate magnon spin current whose direction of magnon flow and direction of spin polarization would not be obvious without carrying the detailed numerical calculation. When the electric field is applied in the high-symmetry points,  $\Gamma K$  ( $\mathbf{x}$ ) and  $\Gamma M$  ( $\mathbf{y}$ ), as shown in Fig. 2(a), we can readily determine the directions of the magnon flow and magnon spin from symmetry analysis. For the  $\Gamma K$  axis, the magnon spin is always perpendicular to the momentum, while for the  $\Gamma M$  axis, they are parallel. Therefore with the electric field applied in the  $\Gamma K$  direction, the magnon spin conductivity tensor has off-diagonal terms, which means that the magnon spin current flowing in the  $\mathbf{x}$  direction is polarized in the  $\mathbf{y}$  direction ( $\sigma_{xx}^y$ ), while for the flowing direction in the  $\mathbf{y}$  direction the magnon spin current is polarized in the  $\mathbf{x}$  direction ( $\sigma_{yy}^x$ ). As for the situation where the field is applied in the  $\Gamma M$  direction, the polarization of the magnon spin current is always in the same direction as the flow direction. In other words, the magnon spin conductivity tensor is diagonal with the  $\sigma_{xx}^x$  and  $\sigma_{yy}^y$  components. This symmetry dictated behavior of the magnon spin conductivity tensor also has been found in spin-polarized charge currents in such systems [35]. This unique anisotropic magnon spin current makes noncollinear AFMs a more interesting system in the study of charge-spin conversion in zero magnetic field as compared to the usual Rashba spin-orbit coupling induced phenomena.

One of the major differences between electron spin current and magnon spin current is that the latter is highly temperature dependent. Two major reasons make the temperature essential: the number of magnons increases with the temperature, and the electron-magnon scattering involves inelastic processes that require the thermal energy to be effective. Mathematically, the temperature appears in the equilibrium magnon number, Eq. (11), and the scattering term, Eq. (12). In addition to the magnon spin conductivity, we further define magnon spin Hall angle (SHA) as  $(e/\hbar)[(\sigma_m)_{jk}^i/(\sigma_e)_{kk}]$  where  $\sigma_e$  is the electron electric conductivity, to compare the electric field driven magnon spin current in noncollinear antiferromagnetic metals to the conventional spin Hall effect in nonmagnetic metals. We show the magnon spin



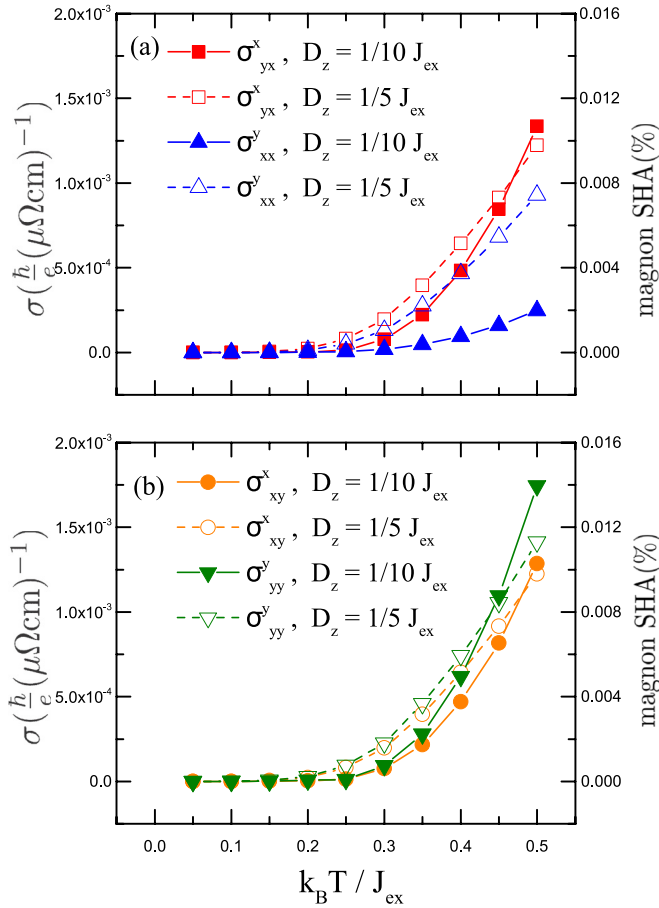


FIG. 3. Temperature dependence of magnon spin conductivity and magnon SHA for charge current flowing in the  $\Gamma K$  (a) or the  $\Gamma M$  (b) direction at two DMI conditions. Material parameters are as follows: electric resistivity for electron  $\rho_e = 320 \mu\Omega \text{ cm}$  [18],  $J_{sd} = 1 \text{ meV}$ , and  $\tau_v = 10^{-6} \text{ s}$ . Note that for the parameters used in the figure, e.g.,  $J_{ex} = 10 \text{ meV}$ ,  $D_z = 1/10 J_{ex}$ , and  $K = 1/1000 J_{ex}$ , the number of magnons in three bands at the highest temperature,  $k_B T / J_{ex} = 0.5$ , remain small—0.9% for the red band, 3.7% for the green band, and 6.7% for the blue band per site—indicating the validity of the linear spin-wave approximation we used in the paper.

conductivity and magnon SHA as a function of temperature in Fig. 3 with field applied either in the  $\Gamma K$  [Fig. 3(a)] or the  $\Gamma M$  [Fig. 3(b)] direction. Both longitudinal and transverse magnon spin conductivities vanish at low temperatures.

#### IV. DISCUSSIONS AND CONCLUSIONS

In a nonmagnetic or collinear antiferromagnetic metal, one would think that the spin current only exists through

the spin Hall effect in which the spin-orbit coupling is required. We show in this paper that the magnon spin current in a noncollinear antiferromagnetic metal is naturally present even though there is no net magnetization and there is no external spin current injection into the AFM. Two essential mechanisms are responsible for the magnon spin current: the magnon spectra have spin-momentum locking characteristics, and the electron-magnon scattering transfers momentum from conduction electrons to the magnons. Due to complex spin-momentum locking patterns, the resulting magnon spin current tensor is rather difficult to predict for an applied electric field in an arbitrary direction relative to the lattice orientation. In the case of the electric field applied in the direction with the high-symmetry points,  $K$  and  $M$ , the direction of the magnon spin current could be immediately determined by symmetry analysis.

We wish to briefly compare the magnon spin current generated by a thermal gradient. In a collinear AFM, the thermal gradient would not generate any net magnon spin current because the thermal gradient leads to a net magnon momentum, and since there is no spin-momentum dependence, the resulting sum over the spin of the degenerated magnons remains zero. In noncollinear AFMs, the magnon bands can have a nonzero Berry curvature. The connection between the magnon conductance and Berry curvature of the magnon bands has been theoretically studied [36–38] and the magnon Hall current is an intrinsic mechanism, i.e., the magnon conductance is independent of the relaxation, in contrast to the extrinsic mechanism we discussed here. Similar to the electron transport, it remains unclear for a given material which mechanism dominates. As for the symmetry properties of the magnon current tensor, these two mechanisms give identical results since the underlying crystal and magnetic symmetries are the same. One important difference is that our formalism applies to antiferromagnetic metals where the electric current is the source of magnon current, while in the previous studies on magnon Seebeck effect, the focus was on magnetic insulators [23].

Magnon spin current may not be directly measurable in the bulk films. As in the measurement for the electron spin current, one needs an additional contact layer that may support magnon accumulation or give rise to a magnetic torque. The detailed discussion on the possible experimental realization of the magnon spin torques is beyond the scope of the present paper.

#### ACKNOWLEDGMENT

This work was partially supported by the U.S. National Science Foundation under Grant No. ECCS-1708180.

- [1] T. Jungwirth, X. Marti, P. Wadley, and J. Wunderlich, *Nat. Nanotechnol.* **11**, 231 (2016).
- [2] V. Baltz, A. Manchon, M. Tsoi, T. Moriyama, T. Ono, and Y. Tserkovnyak, *Rev. Mod. Phys.* **90**, 015005 (2018).

- [3] T. Jungwirth, J. Sinova, A. Manchon, X. Marti, J. Wunderlich, and C. Felser, *Nat. Phys.* **14**, 200 (2018).
- [4] A. Manchon, J. Železný, I. M. Miron, T. Jungwirth, J. Sinova, A. Thiaville, K. Garello, and P. Gambardella, *Rev. Mod. Phys.* **91**, 035004 (2019).

- [5] Y. Ohnuma, H. Adachi, E. Saitoh, and S. Maekawa, *Phys. Rev. B* **87**, 014423 (2013).
- [6] S. M. Rezende, R. L. Rodríguez-Suárez, and A. Azevedo, *Phys. Rev. B* **93**, 014425 (2016).
- [7] S. M. Wu, W. Zhang, A. KC, P. Borisov, J. E. Pearson, J. S. Jiang, D. Lederman, A. Hoffmann, and A. Bhattacharya, *Phys. Rev. Lett.* **116**, 097204 (2016).
- [8] W. Lin, K. Chen, S. Zhang, and C. L. Chien, *Phys. Rev. Lett.* **116**, 186601 (2016).
- [9] R. Cheng, J. Xiao, Q. Niu, and A. Brataas, *Phys. Rev. Lett.* **113**, 057601 (2014).
- [10] H. Wang, C. Du, P. C. Hammel, and F. Yang, *Phys. Rev. Lett.* **113**, 097202 (2014).
- [11] Y. Cheng, K. Chen, and S. Zhang, *Appl. Phys. Lett.* **112**, 052405 (2018).
- [12] R. Cheng, D. Xiao, and J.-G. Zhu, *Phys. Rev. B* **98**, 020408(R) (2018).
- [13] Y. Wang, D. Zhu, Y. Yang, K. Lee, R. Mishra, G. Go, S.-H. Oh, D.-H. Kim, K. Cai, E. Liu, S. D. Pollard, S. Shi, J. Lee, K. L. Teo, Y. Wu, K.-J. Lee, and H. Yang, *Science* **366**, 1125 (2019).
- [14] W. Zhang, M. B. Jungfleisch, W. Jiang, J. E. Pearson, A. Hoffmann, F. Freimuth, and Y. Mokrousov, *Phys. Rev. Lett.* **113**, 196602 (2014).
- [15] Y. Ou, S. Shi, D. C. Ralph, and R. A. Buhrman, *Phys. Rev. B* **93**, 220405(R) (2016).
- [16] H. Chen, Q. Niu, and A. H. MacDonald, *Phys. Rev. Lett.* **112**, 017205 (2014).
- [17] J. Kübler and C. Felser, *Europhys. Lett.* **108**, 67001 (2014).
- [18] S. Nakatsuji, N. Kiyohara, and T. Higo, *Nature (London)* **527**, 212 (2015).
- [19] A. K. Nayak, J. E. Fischer, Y. Sun, B. Yan, J. Karel, A. C. Komarek, C. Shekhar, N. Kumar, W. Schnelle, J. Kübler, C. Felser, and S. S. P. Parkin, *Sci. Adv.* **2**, e1501870 (2016).
- [20] B. Flebus, Y. Tserkovnyak, and G. A. Fiete, *Phys. Rev. B* **99**, 224410 (2019).
- [21] A. Mook, J. Henk, and I. Mertig, *Phys. Rev. B* **99**, 014427 (2019).
- [22] K.-S. Kim, K. H. Lee, S. B. Chung, and J.-G. Park, *Phys. Rev. B* **100**, 064412 (2019).
- [23] A. Mook, R. R. Neumann, J. Henk, and I. Mertig, *Phys. Rev. B* **100**, 100401(R) (2019).
- [24] M. Kimata, H. Chen, K. Kondou, S. Sugimoto, P. K. Muduli, M. Ikhlas, Y. Omori, T. Tomita, A. H. MacDonald, S. Nakatsuji, and Y. Otani, *Nature (London)* **565**, 627 (2019).
- [25] P. K. Muduli, T. Higo, T. Nishikawa, D. Qu, H. Isshiki, K. Kondou, D. Nishio-Hamane, S. Nakatsuji, and Y. C. Otani, *Phys. Rev. B* **99**, 184425 (2019).
- [26] N. Okuma, *Phys. Rev. Lett.* **119**, 107205 (2017).
- [27] Y. Cheng, K. Chen, and S. Zhang, *Phys. Rev. B* **96**, 024449 (2017).
- [28] M. Elhajal, B. Canals, and C. Lacroix, *Phys. Rev. B* **66**, 014422 (2002).
- [29] T. Yildirim and A. B. Harris, *Phys. Rev. B* **73**, 214446 (2006).
- [30] K. Matan, D. Grohol, D. G. Nocera, T. Yildirim, A. B. Harris, S. H. Lee, S. E. Nagler, and Y. S. Lee, *Phys. Rev. Lett.* **96**, 247201 (2006).
- [31] N. D. Mermin and H. Wagner, *Phys. Rev. Lett.* **17**, 1133 (1966).
- [32] J. H. P. Colpa, *Phys. A (Amsterdam, Neth.)* **93**, 327 (1978).
- [33] S. S.-L. Zhang and S. Zhang, *Phys. Rev. Lett.* **109**, 096603 (2012).
- [34] R. Schmidt, F. Wilken, T. S. Nunner, and P. W. Brouwer, *Phys. Rev. B* **98**, 134421 (2018).
- [35] J. Železný, Y. Zhang, C. Felser, and B. Yan, *Phys. Rev. Lett.* **119**, 187204 (2017).
- [36] H. Katsura, N. Nagaosa, and P. A. Lee, *Phys. Rev. Lett.* **104**, 066403 (2010).
- [37] S. A. Owerre, *Phys. Rev. B* **94**, 094405 (2016).
- [38] S. A. Owerre, *Phys. Rev. B* **95**, 014422 (2017).